Catalytic Carbon Nanostructures and Novel Nanocomposites for Hydrogen Storage

Ashley C. Stowe[a], Joseph A. Teprovich, Jr.[a], Douglas A. Knight[a], Matthew S. Wellons[a] and Ragaiy Zidan*[a]

[a] *Energy Security Directorate, Savannah River National Laboratory Aiken SC 29808.*

[*] *corresponding author. Ragaiy.zidan@srnl.doe.gov; 803-646-8876.*

This article reviews and discusses research activities and results of our studies on catalytic carbon nanostructures and the formation of novel nanocomposites that can reversibly store hydrogen. Carbon nanomaterials have been utilized as catalysts, additives, agents for ball milling and scaffolds, in conjunction with hydrides and complex metal hydrides and have shown remarkable hydrogen interaction properties. Among several nanostructures investigated, buckminster fullerene (C_{60}) has been shown to be an excellent catalyst for hydrogen desorption when added to $NaAlH_4$, $LiAlH_4$ and $LiBH_4$. In the $NaAlH_4/C_{60}$ mixture, it was found that addition of C_{60} lowered the dehydriding temperature and rendered $NaAlH_4$ reversible with hydrogen capacity of 4.3 wt %. A fullerene–$LiBH_4$ composite demonstrates catalytic properties with not only lowered hydrogen desorption temperatures, but also rehydrogenation at a relatively low temperature of 350 °C. A reversible hydrogen capacity of 4.0 wt % was observed over multiple cycles. At higher fullerene content in composites comprised of C_{60} with $NaAlH_4$ or $LiAlH_4$ hydrogen desorbed at lower temperature. Thermolysis results in the formation of alkali metal fullerides and aluminum metal along with hydrogen release. The as-prepared composites of C_{60} with $NaAlH_4$ or $LiAlH_4$ exhibit rapid hydrogen desorption at onset temperatures of 130 ºC and 150 ºC, releasing 2.2 and 5.9 wt % hydrogen, respectively, relative to the composite. The resultant alkali metal fulleride containing composites were found to be capable of reversible hydrogen storage. A series of desorption and absorption experiments on the Na-C_{60} and Li-C_{60} based composites demonstrate a 1.5 wt % and 1.2 wt % reversible capacity, respectively. The complex metal hydride-C_{60} systems were characterized by PCT, XRD, FT-IR, and TGA-RGA. The formation of metal-fulleride materials—similar to traditional hydrofullerenes—appear to be responsible for the observed reversible hydrogen storage.

Introduction

In recent years, development of a hydrogen based fuel economy has received significant interest. This eventual hydrogen economy will require efficient technologies for hydrogen production, storage, and delivery[1]. Hydrogen storage is considered one of the challenges because hydrogen must be stored safely until needed, and then released with minimal energy loses. Realizing the hydrogen economy for transportation applications require developing cost-effective materials that store and release hydrogen with large gravimetric and volumetric densities under moderate thermodynamic conditions[1-2].

Hydrogen can be stored in a number of states: (i) compressed gas, (ii) cryogenic liquid, or (iii) as a component of a solid chemical matrix. The technical challenges faced include storage system, cost, safety, hydrogen densities (both gravimetric and volumetric), sustainability of the fuel component source, accessibility and efficiency of H_2 "on demand", and purity of H_2 stream[1]. Compressed gas allows for immediate hydrogen liberation at a low cost, but is volumetrically very inefficient. Liquid hydrogen is volumetrically very compact, but at a high cost of liquefaction. Solid state chemical storage of hydrogen can be compact and safe, but the added mass of the other chemical constituents must be minimized. Future hydrogen storage systems must have both high volumetric (≥82g H_2 L^{-1}) and gravimetric (≥90 g H_2 kg^{-1}) densities of deliverable hydrogen to meet 2015 U.S. Department of Energy targets[3]. Furthermore, these systems must release hydrogen at significant rates near 85-100 ^oC, which is the temperature provided by the waste heat from a proton exchange membrane (PEM) fuel cell, to enhance efficiencies for use in transportation applications.

Significant progress has been made in solide state hydrogen storage with the discovery of novel chemical hydrides, complex metal hydrides, and adsorption substrates[4]. Chemical hydrides typically offer the largest theoretical gravimetric hydrogen capacities, however, none of these materials have been shown to be reversible. Autrey *et al.* recently reported that mechanical milling of alkali metal hydrides with ammonia borane can further lower the decomposition temperature[5]. This group also showed that incorporation of ammonia borane within both a silica[6] and carbonaceous[7] mesoporous scaffold enhanced the desorption properties by limiting the particle size of NH_3BH_3. This *nano*-ammonia borane releases hydrogen with a near thermoneutral enthalpy. A method has recently been reported which digests spent fuel and chemically regenerates ammonia borane by a detailed chemical synthesis[8], however, on-board refueling is not possible.

Complex metal hydrides—similar to interstitual metal hydrides—involve dissolution of hydrogen into a metal lattice. As the concentration of hydrogen in the lattice grows, metal hydrogen bonds form and the molecular structure is transformed into a metal hydride[9]. One of the most promising

materials, sodium aluminum hydride ($NaAlH_4$) is the most widely studied complex metal hydride material. The kinetics of hydrogen uptake and release of these materials are such that catalysts are needed to improve the reaction rates. Bogdanovic and Schwickardi first demonstrated the catalytic effect of $TiCl_3$ rendering $NaAlH_4$ reversible. Hydrogen desorbed at lower temperatures and with faster kinetics. This material was then rehydrided with the application of a hydrogen overpressure[10]. This has led to optimism that alanates may be suitable materials for hydrogen storage. Extensive research into the catalytic effects of many early transition metals suggest Ti is the most ideal additive for enhanced hydrogen storage properties[11-15]. Despite an intense focus on Ti-catalyzed hydrogen sorption of $NaAlH_4$, a fundamental understanding of how this catalyst works has not been agreed on[16-19]. The presence of NaCl and traces of Ti/Al alloys have been detected, implying that the molecular Ti precursor has taken part in a chemical reaction. It is widely believed that a fundamental understanding of how the catalyst works may help in the rational design of new catalysts for the alanates as well as for other complex hydrides (e.g., borohydrides and amides).

Several groups have investigated the use of carbon materials as possible catalysts for $NaAlH_4$[20-24]. In all cases, the sorption properties of $NaAlH_4$ was enhanced, although the mangitude of the effect varied widely. The catalytic effect is believed to be either through nano-sizing or closer contact with carbon nanostructures. The carbon additives were postulated to be catalysts, however, $NaAlH_4$ and the carbon structures were comixed by balling milling. Tao *et al.*[25] as well as Pierard *et al.*[26] have both shown degradation of the fragile carbon nanostructures due to the significant mechanical energy imparted on the system during ball-milling. Further, mechanical milling is known to introduce Fe contamination from the ball mill vial and/or milling balls[27-28], into the hydrogen storage media which can potentially catalyze the reaction (Fe is an excellent catalyst for dehydrogenation of $NaAlH_4$[29]).

In order to deconvolute the catalytic enhancements of carbon materials from transitional metal inpurities with regard to hydrogensorption properties, intimate mixing of the carbnaceous substrate with a hydrogen storage material has been achieved by solvent based intercaltion[30-32]. Further, a variety of carbon based materials were investigated including, graphite, carbon nanotubes, and fullerenes to optimize the catalytic effect[32]. Similar results have been observed for the carbon/$LiBH_4$ nanocomposite[30]. Fullerene (C_{60}) was found to be the best catalyst for all hydrogen storage materials prepared.

The present review will focus on the role of carbonaceous materials in catalyzing hydrogen sorption from alanate and borohydride materials and the formation of nanocomposites. Further, the mechanism of observed reversibility will be discussed.

Materials and Experiments

Alkali metal fullerides capable of reversible hydrogen absorption/desorption have been synthesized and characterized for their structural and hydrogen sorption properties. The materials were prepared by combination of a carbon additive (SWNT, graphite, C_{60}) and complex metal hydrides by a solvent preparation technique to intimately mix $NaAlH_4$, $LiBH_4$, or $LiAlH_4$ and the carbon nanostructure without introducing metal contaminants (i.e. ball milling). A control sample of Ti-catalyzed $NaAlH_4$ was also prepared. Chemicals were used as provided by the supplier and are listed by supplier as follows. Acros: THF (anhydrous, ≥99.9 %, inhibitor-free), Benzene (anhydrous). Sigma-Aldrich: graphite (99%), 8-50 nm carbon nanotubes(99 %), C_{60} (99.5 %), $LiBH_4$ (hydrogen storage grade), $LiAlH_4$ (95%), and $NaAlH_4$ (hydrogen storage grade). All chemicals were stored and handled under an argon atmosphere in a Vacuum Atmospheres glovebox.

Samples were prepared by combining a carbon nanostructure and the respective complex metal hydride with either THF or benzene. The mixture was stirred with a teflon coated magnetic stir bar for 12 hr. The solvent was removed under reduced pressure and the remaining solids collected. The $LiAlH_4$ composite was prepared in a 60:1 mol ratio ($LiAlH_4$:C_{60}) which is equivalent to the composite containing 76 wt % $LiAlH_4$. The fullerene-$NaAlH_4$ composite was prepared with a 6:1 ratio of $NaAlH_4$:C_{60}. A 60:1 mol ratio of $LiBH_4$:C_{60} was also investigated.

The hydrogen desorption/absorption properties of the material were measured on a HyEnergy PCT Pro 2000 instrument. The PCT vessel and sample were heated at a rate of 2 ^oC/min from room temperature (RT) to 300 or 380 ^oC followed with an isotherm, during which an increase in pressure attributed to the evolution of H_2 was observed. After desorption, the sample was evacuated and allowed to cool to RT before the absorption cycle was started. For the absorption the sample was first charged with 105-120 bar H_2, and then heated to 250 ^oC, followed by a 9-12 hr isotherm at 250 ^oC. Subsequent reversible hydrogen cycling was conducted with identical parameters.

For TGA-RGA experiments a Perkin Elmer Thermogravimetric Analyzer-Pyris 1 TGA was used within an inert glovebox. The sample was heated from 30 to 550 ^oC at heating rate of 2-5 ^oC/min, with a sample size of ~5 mg, The gas released during the heating process was identified by a Hiden Analytical RGA. X-ray powder diffraction (XRD) was used to characterize the products, using Cu-K radiation. During X-ray analysis the samples were protected with a Mylar film to minimize oxidation. Samples analyzed by FT-IR were prepared as KBr pellets in an Argon glovebox and were analyzed on a Jasco FTIR 6300 with a stream of nitrogen purging the sample chamber.

Results and Discussions

Screening of carbon nanostructures as catalysts was performed via computational modeling and corresponding experimental analysis. Fullerene (C_{60}), carbon nanotubes, and graphene are models of zero, one, and two-dimensional carbon nanostructures, and their chemistry can be manipulated by changing their curvature and dimensionality. Changes in curvature of CNT can also have catalytic effects due to localization/delocalization of electrons.

Theoretical calculations show that the geometrical parameters of CNTs deviate from the values obtained from simple wrapping of a perfect hexagonal sheet. The radial breathing mode frequency does not follow the usually assumed 1/d behavior and there is a general softening with the increase of curvature; thus the deviation from the expected behavior

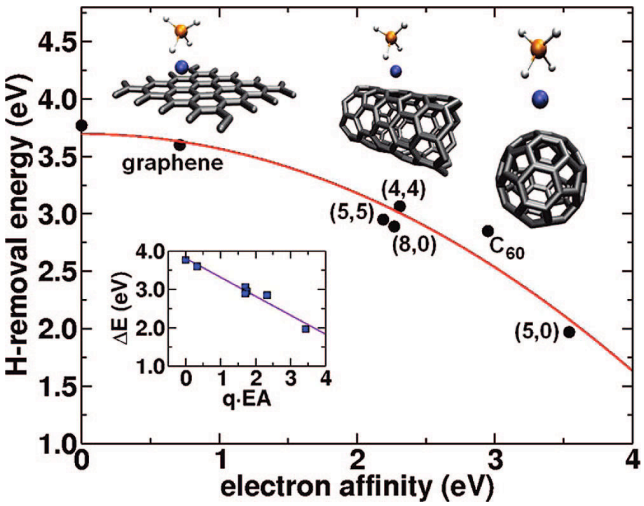

Fig. 1 Correlation of the carbon substrate electron affinity and the hydrogen removal energy. Black circles are ab initio results for H-removal energy as a function of electron affinity (EA) of the carbon substrate. The red curve is a fit of the data with a quadratic function. The inset below the red curve shows the linear relationship between the H-removal energy (ΔE) to the product of transferred charge (q) and EA. The inset above the red curve displays the equilibrium configurations for $NaAlH_4$ interacting with a graphene sheet, (5,0) zigzag carbon nanotube, and fullerene. Na atoms are shown as blue spheres, Al in gold, C in dark gray, and H in white.[32]

increases with increasing curvature. The lattice constant along the tube axis also exhibits a slight shrinking when compared to bulk graphite[33].

First-principles calculations show that the energies needed to remove a hydrogen atom from $NaAlH_4$ supported on a (5,0) carbon nanotube or C_{60} are significantly smaller than those in pure sodium alanate and are nearly the same as when Ti is substituted at the Na site in sodium alanate. Interestingly, no structural changes of the carbon nanostructures take place, and unlike $TiCl_3$, the carbon nanotubes and fullerenes behave as true catalysts. The results can be explained in very simple terms by using the chemistry of the carbon substrates and that of the $NaAlH_4$ cluster. Note that the $NaAlH_4$ cluster is stabilized by the formation of the AlH_4^- anion, charge balanced with sodium in the cationic form. As $NaAlH_4$ interacts with a substrate that is similarly electronegative as AlH_4, the ability of Na to donate the electron to form the AlH_4^- anion is compromised. Hence the covalent bond between Al and H is weakened. This weakening of the metal-hydrogen bond leads to lowering of the hydrogen desorption energy resulting in improved kinetics. The most effective carbonaceous catalysts were then incorporated into a variety of complex metal hydrides for more extensive analysis.

Modeling Results.

Sodium alanate was chosen as the model hydrogen storage material for studying the interaction of carbon structures computationally. A single $NaAlH_4$ formula unit was modeled on the carbon substrate as described in earlier theoretical and experimental results. It has been demonstrated that very small clusters can mimic the properties of their crystals if the latter are characterized by strong covalent or ionic bonds such as those in TiN[34], NaCl[35], Sb_2O_5[36], and W_2O_3[37].

In work by Berseth *et al.* different carbon nanomaterials were considered; zero-, one- and two-dimensional, namely graphene, C_{60}, and singlewalled carbon nanotubes of (5,0), (4,4), (5,5), and (8,0) type. The diameters of the (5,0), (4,4), (5,5), and (8,0) nanotubes were respectively 3.92, 5.43, 6.78, and 6.27 Å. The $NaAlH_4$ cluster was found to preferably bind with the Na atom facing toward the carbon substrates. Figure 3 provides the equilibrium geometry of the $NaAlH_4$ cluster supported on the (5,0) carbon nanotube (CNT), C_{60}, and graphene. The binding energies of the $NaAlH_4$ cluster to these structures were found to be very small, namely 36, 68, and 93 meV for the (5,0) nanotube, C_{60}, and graphene, respectively. The distance between the Na atom and the carbon substrate were calculated to be of the order of 2.3-2.4 Å. The distances between Na and Al and Al and H were, respectively, 2.8 and 1.6-1.7 Å in all these composites and were almost identical with the corresponding values in the isolated $NaAlH_4$ cluster. The near equality of these bond distances and the low binding energies of the $NaAlH_4$ cluster with the various carbon nanostructures were an indication that they do not chemically react, a property characteristic of a true catalyst.

The calclution showed that substrates, conversely, had a dramatic effect on the hydrogen removal energy. These were calculated using the equation

$$\Delta E = E(C_x/NaAlH_3) + E(H) - E(C_x/NaAlH_4)$$

Here, C_x stands for a given carbon substrate (nanotube, fullerene, or graphene). The calculations of the removal energies required optimizing the geometry of $NaAlH_4$ interacting with various nanostructures. The results are given in Figure 1. The binding energy to remove an H atom from an isolated $NaAlH_4$ cluster was found to be 3.8 eV compared with only 2.0 eV to remove the H atom when $NaAlH_4$ is supported on a (5,0) CNT. The Ti-catalyzed $NaAlH_4$ system has a similar removal energy where Ti replaces the Na atom in a $NaAlH_4$ crystal[38-39].The hydrogen removal energy was shown to vary widely as the carbonaceous support changed with graphite structure having the least effect. These differences were explained through understanding the electron affinities of the carbonaceous nanostructures. The electron affinity was found to depend upon the curvature of the substrate which increases with increasing curvature. C_{60} has a diameter of 7 Å with a large radius of curvature relative to the 8-50 nm diameter of other carbon structures. This was consistent with the hypothesis that increasing the carbon substrate surface curvature results in greater catalytic activity. In addition, as the electron affinity of the substrate decreases, the energy to remove the hydrogen atom also increases.

Comparison of the stability of AlH_n, AlH_n^-, and $NaAlH_n$ clusters (n = 1-4) were shown to indicate that among neutral AlH_n clusters, AlH_3 is the most stable cluster while AlH_4 is unstable. The AlH_4 cluster, however, could be stabilized by adding an extra electron (AlH_4^-). $NaAlH_4$ stability is therefore governed by the charge transfer from Na to AlH_4, transforming the former into a cation and the latter into an anion.

When a metal hydride is co mixed with a carbon substrate, AlH_4 has another competitor for the Na atom electron. When the electron is transferred to the carbon support rather than the AlH_4 unit, the Al-H bond is weakened resulting in lower hydrogen desorption energy. The larger the electron affinity of the substrate, the greater the probability of Na donating its electron to the substrate. The plot of the electron affinity of the

various carbon nanostructures versus the hydrogen removal energy in Figure 1 was found to be best fitted by a parabola where the hydrogen removal energy decreased as the electron affinity of the substrate increased. This relationship may be understood as follows. Once the hydrogen atom has left the $NaAlH_4$ cluster, the remaining $NaAlH_3$ unit can transfer charge to the carbon support and thus reduce the total energy of the system.

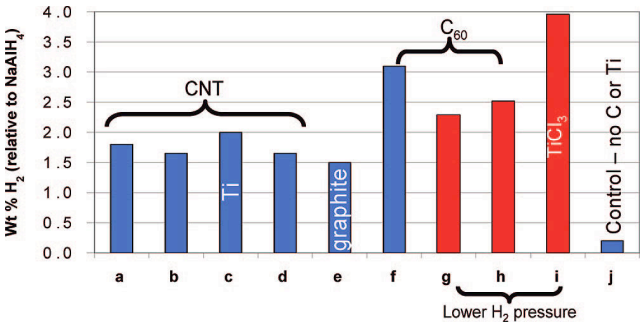

Fig. 2 Screening study results of $NaAlH_4$/carbon mixtures. These values are for hydrogen desorbed on the second desorption cycle. Samples a-f and j we heated up to 280 °C for 3 h, and the absorption step was performed at ~2.1 x 10^7 Pa H_2 and 150 °C. Samples g-I were heated to 350°C for 3 h, and the absorption step was performed at 1.2 x 10^7 Pa H_2 and 150°C. Sample key: (a) 8 nm CNT, (b) 10—20 nm CNT, (c) 10-20 nm CNT with 4 mol% Ti, ((d) 50 nm CNT, (e) graphite, (f) C_{60} (g) C_{60} (h) C_{60}, (i) control no carbon, ball mill 4 mol % $TiCl_3$, and (j) control no carbon or Ti. The two pressures used for the rehydriding step (which affects the amount of hydrogen desorbed in the second cycle) are highlighted by color: high pressure experiments are blue while lower pressure experiments are red.[32]

This *ab initio* studies have shown that the electronegative properties of CNTs and fullerenes could indeed lead to a sufficient reduction in hydrogen binding energies in sodium alanate.

$NaAlH_4$:Carbonaceous support

In Berseth *et al*, mixtures containing recrystallized $NaAlH_4$ within graphite, nanotube, and C_{60} were prepared by solvent addition to avoid the use of ball milling and prevent degradation and creation of defect sites in the carbon materials. The results of the hydrogen cycling screening test are summarized in Figure 2. These results are from the second desorption cycle to avoid recording possible residual solvent contributed to the first desorption cycle. In all cases, reversibility is observed (recall that uncatalyzed $NaAlH_4$ is not reversible), and each carbon nanostructure enhances desorption. C_{60} is the best carbon additive for $NaAlH_4$, rehydriding $NaAlH_4$ to 4.3 wt % over 8 h with ~2.1× 10^7 Pa H_2 pressure.

Fullerence, which has the greatest curvature, showed the reatest catalytic effect as predicted by the *ab initio* calculations. Carbon nanotubes are graphitic carbon sheets rolled into tubes, and it is possible that the accelerated absorption relative to flat graphite particles is due in part to the changes in the π- and σ-bonding orbitals that the H_2 molecules interact with on the surface of the material.

$NaAlH_4$:C_{60}

In work reported by Teprovich *et al*, TGA-RGA results (Figure 3), indicated $NaAlH_4$:C_{60} (6:1) mixture undergoes thermal decomposition in a temperature range similar to previous studies of catalyzed $NaAlH_4$. The initial loss of 0.3 wt. % is the loss of trace amounts of benzene remaining from the composite solvent mixing process and is confirmed by RGA analysis. The decomposition of the $NaAlH_4$:C_{60} (6:1) occured over a 180 - 230 °C temperature range with approximately a 2.2 wt % loss indicative of a complete transition to Na, Al, C and H_2 gas. The observed mass loss is consistent with a calculated mass loss of 2.3 wt. % for an idealized 6:1 $NaAlH_4$:C_{60} composite which is completely dehydrided—including NaH. The thermal decomposition of NaH below 230 °C is unprecedented. Most $NaAlH_4$ desorption studies report NaH as the final product. TPD measurements indicate a two step desorption in which $NaAlH_4$ decomposed to NaH, Al, and H_2 followed by NaH decomposition. This observation was surpsingly different from the traditional decomposition chemistry of $NaAlH_4$ which involves a hexavalent Na_3AlH_6 intermediate. Rehydrogenation of the decomposed $NaAlH_4$:C_{60} material with 120 bar H_2 at 250 °C resulted in hydrogen uptake. The subsequent desorption experiment showed a single desorption of 1.5 wt. % H_2 at 150 °C. This "partial" rehydrogenation/dehydrogenation of the composite mimicking the reversibility reported for $NaAlH_4$ is instead likely due to the formation of a new material: *sodium fulleride nano composite*.

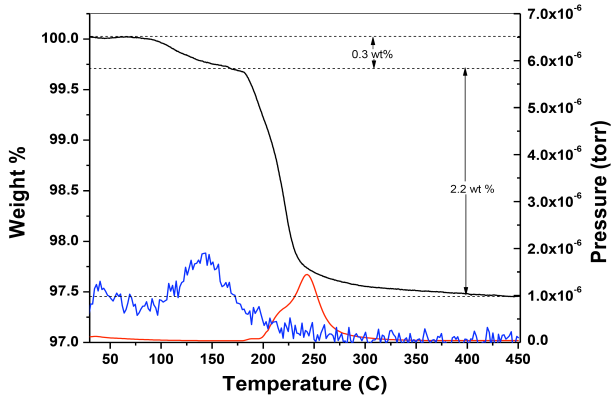

Fig. 3 TGA-RGA of the $NaAlH_4$:C_{60} composite (black) shows only a 0.3 wt. % loss due to benzene (blue). The RGA signal for benzene was multiplied by 500 to fit on the scale of the graph. Hydrogen (red) release corresponds to the weight loss observed in the TGA.[31]

$LiAlH_4$:C_{60}

The $LiAlH_4$:C_{60} mixture was synthesized with a molar ratio of 60:1 and was subject to the same hydrogen desorption/absorption conditions. $LiAlH_4$ decomposes through three steps with 5.3, 2.6, and 2.6 wt % H_2 released during each step, respectively. The final desorption step involving LiH dehydrogenation typically occurs above 680 °C and is not practical under experimental conditions of interest. This limits the available hydrogen content of $LiAlH_4$ to 7.9 wt %. Figure 4 shows the $LiAlH_4$:C_{60} desorption results for a series of hydrogenation/dehydrogenation cycles. Three distinct desorption events were observed, indicating that all three desorption reactions (including LiH dehydrogenation) occurred and released 5.9 wt% hydrogen with respect to the total composite weight. Further, the initial desorption event occurs approximately 20 °C lower in temperature than pure $LiAlH_4$.

Subsequent absorption and desorption cycles were performed and showed that the material can reversibly store 1.2 wt% hydrogen. However, the release of hydrogen in the second

and third desorption does not occur until ~260 °C (orange and green curves in Fidure 4). Desorption of pure $LiAlH_4$ releases 7.5 wt % in two distinct desorption events at 150 and 175 °C. Subsequent rehydrogenation of $LiAlH_4$ was unsuccessful, as expected.

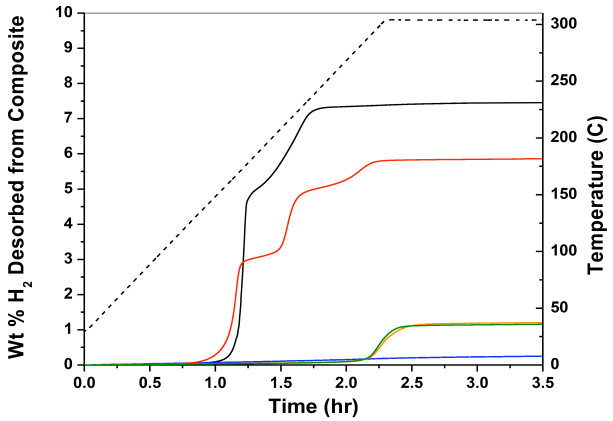

Fig. 4 TPD of pure $LiAlH_4$ (black- 1st desorption, blue- 2nd desorption), $LiAlH_4$:C_{60} (red- 1st desorption, green- 2nd desorption, orange- 3rd desorption). Dashed line is the sample temperature. Heating rate was 2 °C/min.[31]

This data again suggested that the material being regenerated during the absorption process is not $LiAlH_4$, but a *lithium-fulleride nano-composite.*

$LiBH_4$:C_{60}

Wellons *et al* reported results of a $LiBH_4$:C_{60} mixture with a mole ratio of 60:1 showing hydrogen desorption profiles depected in figure 5.[30] Figure 5 shows hydrogen desorption as a function of time from as prepared mixture and after the first three hydrogenation cycles. Similar to the alanate-fullerene systems, C_{60} lowers the desorption temperature compared to pure $LiBH_4$. The hydrogen desorption temperature of the $LiBH_4$:C_{60} composite is lowered by 80 °C °C to *ca* 320 °C (compared to ca 400 °C in uncatalyzed $LiBH_4$). Further, presence of the C_{60} additive results in a reversible hydrogen absorption capacity of 4.2 wt % over 12 h under 1.2×10^7 Pa H_2 pressure and 350 °C. Subsequent hydrogen desorption measurements after composite regeneration show only slight degradation of the reversible hydrogen storage capacity, with 4.0 wt % rehydriding. The decrease in capacity is likely due to the formation of small quantities of non-reversible lithium borohydride intermediates (e.g. LiB_xH_y) and/or the formation of diborane during the hydrogenation and dehydrogenation cycles.

To better understand the catalytic effects of C_{60} on $LiBH_4$ as well as the cyclic degradation of the composite materials, Wellons *et al* performed preliminary phase analyses. X-ray diffraction (XRD) measurements of the as-prepared, dehydrided, and rehydrided $LiBH_4$:C_{60} mixture revealed only the presence of crystalline $LiBH_4$ in the as-prepared mixture. The lack of a characteristic fullerene x-ray pattern is consistent with an intimate mixture of the fullerene and $LiBH_4$, and the formation of a homogeneous C_{60} distribution. The dehydrided composite scan showed no crystalline material and the rehydrided composite scan showed the reemergence of $LiBH_4$, indicating a regeneration of the complex metal hydride. This is a departure from the alanate-fullerene mixtures discussed previously which form metal-fulleride nano-composites. A minor amount of LiH was also observed in the rehydrided mixture suggesting that a volatile boron-containing species (i. e. B_2H_6) is forming which will reduce the boron content in the mixture over multiple cycles.

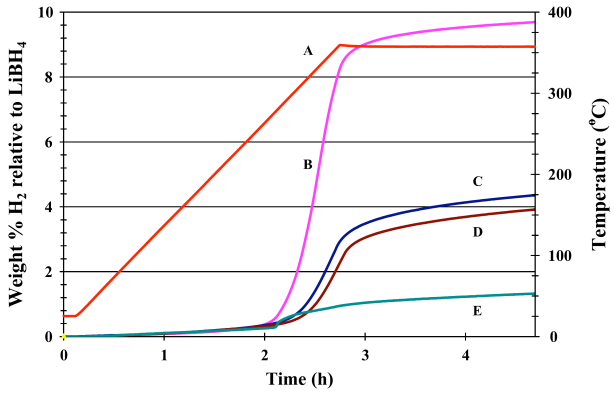

Fig. 5 TPD curves for the $LiBH_4$:C_{60} mixture: first desorption (B), second desorption (C), and third desorption (D). The temperature gradient (A) increased at 2 °C min^{-1} and held at a 350 °C isotherm. Hydrogen reabsorption was done with 1.2×10^7 Pa H_2 at 350 °C for 12 h. Control TPD of as-received $LiBH_4$ is represented by (E).[30]

Metal-fullerides (M_xC_{60})

Work reported by Teprovich *et al* showed thermal decomposition of alanate:C_{60} mixtures to result in incorporation of the metal cation into the fullerene lattice via metal-carbon bond formation.[31] The new storage material has been identified as a *metal-fulleride nano-composite* ($M_xC_{60}H_y$). XRD scans of the resultant dehydrogenated and hydrogenated alanate:C_{60} material shows a powder diffraction pattern which matches the known Na_6C_{60} fulleride[40] and residual Al metal (Figure 6).

After dehydrogenation of $NaAlH_4$ into Al, H_2, and NaH, sodium hydride (NaH) appears to react with C_{60}. Hydrogen is eliminated as Na atoms are incorporated into the C_{60} structure. No metal hydride species is observed after rehydriding, as evidenced by the lack of a crystalline material in the XRD and FT-IR measurements. The fulleride appears wholly responsible for the observed hydrogen storage reversibility (formation of AlH_3 requires $>10^5$ bar hydrogen overpressure and is unlikely under these conditions). In addition, the rehydrided pattern indicates the aluminum remains metallic during the rehydriding treatment which is consistent with it functioning as a spectator material and not participating in hydrogen sorption. Na_6C_{60} maintains its crystallinity and general spatial structure during soprtion cycles, but the relative decrease in intensity of peaks at 17° and 20° (2θ) likely represents a deformation of structure due to hydrogen incorporation. FT-IR spectroscopy of hydrided and rehydrided Na_6C_{60} show the emergence of C-H stretching vibrations at 3000 cm^{-1} not present within a C_{60} standard exposed to identical absorption conditions. The emergence of these C-H peaks and the C-C stretching peaks at 1427 and 1181 cm^{-1} is consistent with the formation of a hydrofullerene moiety.

The presence of these C-H stretches were evidence the

hydrogen uptake observed is be due to carbon-hydrogen bond formation of hydrofullerene rather than the rehydrogenation or reversal of the $NaAlH_4$ sorption mechanism (Figure 7)[40].

The work reported by Teprovich *et al.*, similarly, showed $Li_xC_{60}H_y$ is formed by decomposition of $LiAlH_4$:C_{60}. This result was supported by theoretical studies[41] of $Li_{12}C_{60}$ by Sun *et al.* predicting the formation of $Li_xC_{60}H_y$. Dehydrogenation of this material (Figure 8) showed two distinct desorption events at ~260 °C (1.2 wt %) and at ~ 350 °C (1.5wt%). Hydrogen was the only evolved gas detected by mass spectrometry.

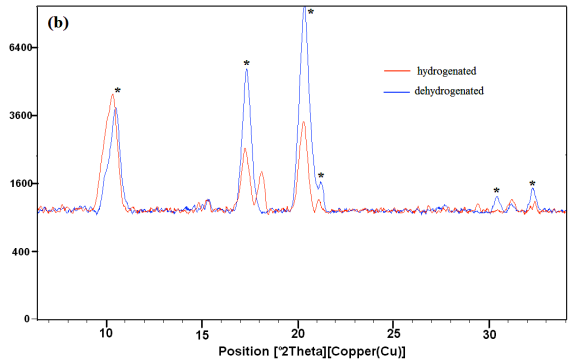

Fig. 6 X-ray powder diffraction of the desorbed and adsorbed $NaAlH_4$:C_{60} material. Identified by * is the Na_6C_{60} material as well as the presence of metallic aluminum as marked by the symbol, Al. A close-up overlap of the hydrogenated (red) and dehydrogenated (blue) material shows only subtle changes as the hydrogen adsorbs into the material [31].

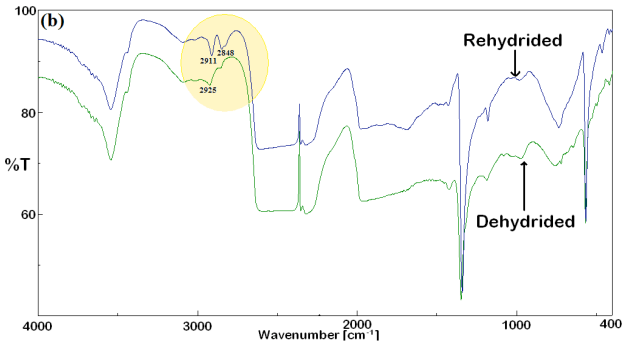

Fig. 7 FT-IR spectroscopy data for the rehydrided Na_6C_{60} material (blue) is placed into comparison with the dehydrided material (green) showing the appearance of C-H stretches (highlighted in yellow) in the hydrogenated material[31].

Unlike the sodium-fulleride system, no XRD reflections were representative of a descrete lithium fulleride material. This could be due to the formation of an amorphous phase. It was apparent, however, that the crystalline nature of C_{60} within the composite is altered when subjected to the high temperatures and hydrogen pressures during cycling. It should also be noted that the $LiAlH_4$:C_{60} mixture used as the precursor for lithium fulleride formation had an initial molar ratio of 60:1, such a large excess of lithium (or $LiAlH_4$) would remain after formation of $Li_xC_{60}H_y$ Interestingly, the two new vibrations appear in the FTIR spectrum of rehydrided $LiAlH_4$:C_{60} at 2911 and 2848 cm^{-1}, consistent with the formation of hydrogenated C_{60}[40]. The emergence of these C-H peaks are consistent with the formation of a hydrofullerene moiety similar to the

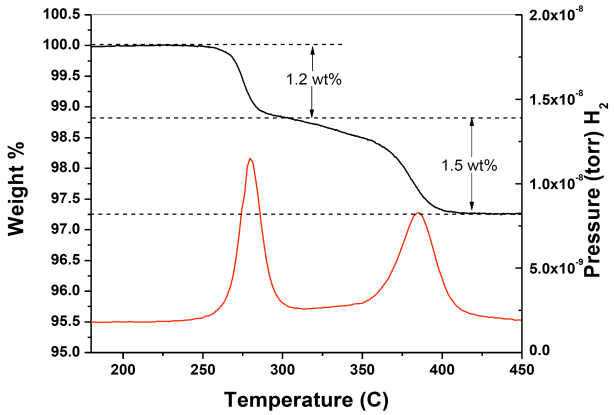

Fig. 8 TGA-RGA plot for $LiAlH_4$:C_{60} after the material was rehydrided twice and shows two distinct desorption events. The weight % determined by the TGA is shown in black and the hydrogen signal from the RGA is shown in red. Heating rate was 2 °C/min[31].

$NaAlH_4$:C_{60} system. The temperatures required for absorption and desorption indicate the hydrogen is incorporated into the composite through chemisorption rather than physisorption to either lithium or carbon atoms or both in the material. The role of the aluminum (if any) has not been determined in either system.

Conclusions

Carbonaceous nanostructures have been shown to catalyze complex metal hydrides resulting in hydrogen gas release at lower temperture than the pure complex metal hydride. Furthermore, reversibility was shown in the borohydride system of 4.0 wt %. Calculations using density functional theory indicate a strong dependence of a carbon supports' electron affinity on its catalytic effectiveness in the alanate systems. As the curvature of the carbon surface increases—correlating with increased electron affinity—there is a greater interaction of the alkali atom with the substrate thereby weakening the Al-H bond in the AlH_4 cluster. As a result, the temperature of hydrogen release is lowered. Computations and the related experiments show fullerene (C_{60}) to be the most effective carbon catalyst for hydrogen desorption. $(Na/Li)_3AlH_6$ is not formed during decomposition of $MAlH_4$:C_{60} mixtures. These mixtures are partially reversible due to the formation of a *metal-fulleride nano-composite* in which the cation is chemically incorporated into the fullerene molecular unit. Characterization of the cycled material indicates the alkali metal fullerides are likely similar in structure and physical properties to hydrofullerenes. Unlike known hydrofullerene materials the present results show fullerides with significantly lower temperatures of hydrogen desorption at 150 and 260 °C (Na and Li, respectively) compared to desorption temperatures of 400 – 500 °C for $C_{60}H_{18}$.

The $LiBH_4$:C_{60} mixture does not appear to undergo the same transformation to lithium fulleride as with the $LiAlH_4$ analog. Rehydriding experiments indicate regeneration of the $LiBH_4$ starting material in high yields. The origin of this difference is not known. It may be that metallic aluminum left over in the alante deconposition plays a vital, but not yet understood role in formation of the *metal-fulleride nano-composite*. Elemental boron is more likely to form volatile bi-products such as

diborane and can be removed from the lattice.

It is important to note that it is possible to dehydrogenate simple metal hydrides (i.e. LiH and NaH), once thought impractical for hydrogen storage, at lower temperature when mixed with carbon nanostructures such as C_{60}.

Further investigation of the $M_xC_{60}H_y$ nano-composite should be explored in order to determine the optimal metal ratio for stable nano-composites which both incorporate large quantities of hydrogen and desorb this hydrogen efficiently at low temperatures.

References

1 Satyapal, S.; Petrovic, J.; Read, C.; Thomas, G.; Ordaz, G. *Catal*. *Today* **2007**, *120* (3-4), 246–256.

2 Ross, D. K. *Vacuum* **2006**, *80* (10), 1084–1089.

3http://www.eere.energy.gov/vehiclesandfuels/about/partnerships/freedomcar.

4 Recent information can be found at: http://www.eere.energy.gov/hydrogenandfuelcells.

5 Z. Xiong, C. Yong, G. Wu, P. Chen, W. Shaw, A. Karkamkar, T. Autrey, M. Jones, S. Johnson, P. Edwards, B. David. *Nature Materials* 2008, **7**, 138.

6 A. Gutowska, L. Li, Y. Shin, C.M. Wang, X.S. Li, J.C. Linehan, R.S. Smith, B.D. Kay, B. Schmid, W. Shaw, M. Gutowski, T. Autrey. *Angew. Chem. Int. Ed.* 2005, **44**, 3578.

7 A. Feaver, S. Sepehri, P. Shamberger, A. Stowe, T. Autrey, G. Cao. *J. Phys. Chem. B Letters* 2007, **111**, 7469.

8 B. Davis, D. Dixon, E. Garner, J. Gordon, M. Matus, B. Scott, F. Stephens. *Angew. Chem., Int. Ed.* 2009, **48**, 6812.

9 Y. Fukai, *The Metal-Hydrogen System*, 2nd Ed. Springer, New York, 2005.

10 B. Bogdanovic, M. Schwickardi. *J. Alloys Compd.* 1997, ***253-254***, 1.

11 Sakintuna, B.; Lamari-Darkrim, F.; Hirscher, M. *Int. J. Hydrogen Energy* **2007**, *32* (9), 1121–1140.

12 Sandrock, G.; Gross, K.; Thomas, G. *J. Alloys Compd.* **2002**, *339* (1-2), 299–308.

13 Anton, D. L. *J. Alloys Compd.* **2002**, *356-357*, 400–404.

14 Zidan, R. A.; Takara, S.; Hee, A. G.; Jensen, C. M. *J. Alloys Compd.* **1999**, *285*, 119–122.

15 Bogdanovic, B.; Felderhoff, M.; Pommerin, A.; Schu¨th, F.; Spielkamp, N. *Adv. Mater.* **2006**, *18* (9), 1198–1201.

16 Balde, C. P.; Stil, H. A.; vanderEerden, A. M. J.; deJong, K. P.; Bitter, J. H. *J. Phys. Chem. C* **2007**, *111* (6), 2797–2802.

17 Haiduc, A. G.; Stil, H. A.; Schwarz, M. A.; Paulus, P.; Geerlings, J. J. C. *J. Alloys Compd.* **2005**, *393* (1-2), 252–263.

18 Majzoub, E. H.; Gross, K. J. *J. Alloys Compd.* **2003**, *356-357*, 363–367.

19 Leon, A.; Kircher, O.; Rosner, H.; Decamps, B.; Leroy, E.; Fichtner, M.; Percheron-Gue´gan, A. *J. Alloys Compd.* **2006**, *414* (1-2), 190–203.

20 Cento, C.; Gislon, P.; Bilgili, M.; Masci, A.; Zheng, Q.; Prosini, P. P. *J. Alloys Compd.* **2007**, *437* (1-2), 360–366.

21 Dehouche, A. L. L.; Grimard, N.; Goyette, J.; Chahine, R. *Nanotechnology* **2005**, *16*, 402–409.

22 Zaluska, A.; Zaluski, L.; Strom-Olsen, J. O. *J. Alloys Compd.* **2000**, *298* (1-2), 125–134.

23 Pukazhselvan, D.; Gupta, B. K.; Srivastava, A.; Srivastava, O. N. *J. Alloys Compd.* **2005**, *403* (1-2), 312–317.

24 Wang, J.; Ebner, A. D.; Ritter, J. A. *J. Phys. Chem. B 2006, 110 (35), 17353–17358.*

25 Tao, Z.; Geng, H.; Yu, K.; Yang, Z.; Wang, Y. Mater. Lett. 2004, 58 (27-28), 3410–3413.

26 Pierard, N.; Fonseca, A.; Colomer, J. F.; Bossuot, C.; Benoit, J. M.; Van Tendeloo, G.; Pirard, J. P.; Nagy, J. B. Carbon 2004, 42 (8-9), 1691–1697.

27 Balema, V. P.; Pecharsky, A. O.; Pecharsky, V. K. J. Alloys Compd. 2000, 307 (1-2), 184–190.

28 Balema, V. P.; Pecharsky, V. K.; Dennis, K. W. J. Alloys Compd. 2000, 313 (1-2), 69–74.

29 Bogdanovic, B.; Brand, R. A.; Marjanovic, A.; Schwickardi, M.; Tolle, J. J. Alloys Compd. 2000, 302 (1-2), 36–58.

30 M. Wellons, P. Berseth, R. Zidan. *Nanotechnology* 2009, **20,** 204022.

31 J. Teprovich, Jr., D. Knight, M. Wellons, R. Zidan. *J. Alloys Compd.* 2010, *in press*

32 P. Berseth, A. Harter, R. Zidan, A. Blomqvist, C. Moyses Araujo, R. Scheicher, R. Ahuja, P. Jena. *Nano Letters* 2009, **9**, 1501.

33 J. Kurti, V. Zolyomi, M. Kertesz, G. Sun. *New J. Phys.* 2003, **5**, 1.

34 Chen, Z. Y.; Castleman, J. A. W. *J. Chem. Phys.* **1993**, *98*, 231–235.

35 Xia, P.; Bloomfield, L. *Phys. ReV. Lett.* **1993**, *70*, 1779–1782.

36 Reddy, B. V.; Jena, P. *Chem. Phys. Lett.* **1998**, *288*, 253–260.

37 Sun, Q.; Rao, B. K.; Jena, P.; Stolic, P.; Gantefor, G.; Castleman, J. A. W. *J. Chem. Phys.* **2004**, *121*, 9417–9422.

38 Arau´jo, C. M.; Ahuja, R.; Osorio Guille´n, J. M.; Jena, P. *Appl. Phys. Lett.* **2005**, *86*, 251913. .

39 Arau´jo, C. M.; Li, S.; Ahuja, R.; Jena, P. *Phys. ReV. B* **2005**, *72*, 165101.

40 S.M. Luzan, F. Cataldo, Y.O. Tsybin, A.V. Talyzin, **J. Phys. Chem. C 2009**, *113* ,13133.

41 Q. Sun, P. Jena, Q. Wang, M. Marquez, *J. Am. Chem. Soc*. **2006**, *128* , 9741